

Anisotropic but nodeless superconducting gap in the presence of spin density wave in iron-pnictide superconductor $\text{NaFe}_{1-x}\text{Co}_x\text{As}$

Q. Q. Ge (葛青亲),¹ Z. R. Ye (叶子荣),¹ M. Xu (徐敏),¹ Y. Zhang (张焱),¹ J. Jiang (姜娟),¹ B. P. Xie (谢斌平),¹ Y. Song (宋宇),² C. L. Zhang (张承林),² Pengcheng Dai (戴鹏程),^{2,3} and D. L. Feng (封东来)^{1,*}

¹State Key Laboratory of Surface Physics, Department of Physics, and Advanced Materials Laboratory, Fudan University, Shanghai 200433, People's Republic of China
²Department of Physics and Astronomy, The University of Tennessee, Knoxville, Tennessee 37996-1200, USA
³Beijing National Laboratory for Condensed Matter Physics, Institute of Physics, Chinese Academy of Sciences, Beijing 100190, China
(Dated: July 28, 2021)

The coexisting regime of spin density wave (SDW) and superconductivity in iron pnictides represents a novel ground state. We have performed high resolution angle-resolved photoemission measurements on $\text{NaFe}_{1-x}\text{Co}_x\text{As}$ ($x = 0.0175$) in this regime and revealed its distinctive electronic structure, which provides some microscopic understandings of its behavior. The SDW signature and the superconducting gap are observed on the same bands, illustrating the intrinsic nature of the coexistence. However, because the SDW and superconductivity are manifested in different parts of the band structure, their competition is non-exclusive. Particularly, we found that the gap distribution is anisotropic and nodeless, in contrast to the isotropic superconducting gap observed in an SDW-free $\text{NaFe}_{1-x}\text{Co}_x\text{As}$ ($x=0.045$), which puts strong constraints on theory.

PACS numbers: 74.25.Jb, 74.70.Xa, 79.60.-i, 71.20.-b

Most unconventional superconductors appear in the vicinity of a certain magnetically ordered phase [1]. Magnetism is suggested to play a critical role in the pairing mechanisms of the cuprates [2], heavy Fermion superconductors [2, 3], and even organic superconductors [4]. For iron-pnictide superconductors, a spin density wave (SDW) phase appears next to the superconducting (SC) phase [5–7], and in some cases, they even coexist [8–13], which gives a unique SC ground state. While the coexisting SDW and SC phases may have significant impact on the SC mechanism [9], much is not clear about the subtle interacting nature between magnetism and superconductivity [14]. In fact, theories based on s^{++} pairing symmetry suggest that there must be nodes in the SC gap in this regime [15] and the coexisting SDW and SC phases cannot be microscopic [9]. On the other hand, theories based on s^{+-} pairing symmetry suggest nodeless SC gap in the presence of weak magnetic order; moreover, the coexistence may cause angular variation of the SC gap, and even give rise to nodes in the limit of strong antiferromagnetic (AFM) ordering [15, 16], as indicated in a thermal conductivity study on $\text{Ba}_{1-x}\text{K}_x\text{Fe}_2\text{As}_2$ [17].

The coexistence of SDW and superconductivity in various iron pnictides has been illustrated by neutron scattering [8–12], nuclear magnetic resonance [18, 19], and angle-resolved photoemission spectroscopy (ARPES) experiments [13]. Recent scanning tunneling microscope (STM) studies show the real-space coexistence and competition of SDW and superconductivity in $\text{NaFe}_{1-x}\text{Co}_x\text{As}$ [20, 21]. However so far, little is known regarding the electronic structure of the coexisting phase in the momentum space, such as its SC gap distribution, and how the two orders coexist and compete on the same electronic structure. In this paper, we report ARPES studies on $\text{NaFe}_{0.9825}\text{Co}_{0.0175}\text{As}$ in this coexisting regime. The band structure reconstruction corresponding to the SDW for-

mation and the SC gap could be observed on the same bands, which provides a direct evidence for the intrinsic coexistence of the two orders. We found that SDW formation does not cause much depletion of the states near the Fermi energy (E_F), therefore, it allows the superconductivity to occur. Moreover, the SC gap distribution is found nodeless on all Fermi surface sheets: it is isotropic on the hole pocket, but it is highly anisotropic on the electron pockets. Our results reveal the distinct electronic properties of the coexisting phase and provide explicit constraints on theory.

High-quality $\text{NaFe}_{0.9825}\text{Co}_{0.0175}\text{As}$ single crystals were synthesized by the self-flux method described elsewhere [22]. The SC transition temperature (T_c) is determined by the magnetic susceptibility measurements with a SQUID magnetometer [Fig. 1(a)], which shows an onset drop at 20.5 K. Resistivity measured by PPMS indicates zero resistivity below 18 K, and a structural transition at $T_S = 36$ K. Our neutron scattering data show that the SDW transition temperature (T_N) is 28 K [Fig. 1(b)]. ARPES data were taken with various photon energies in circular polarization at the 1-Cubed beamline of BESSY II, other photoemission measurements were performed either with 21 eV photons at beamline 5-4 of the Stanford Synchrotron Radiation Laboratory (SSRL), or with randomly polarized 21.2 eV light from an in-house SPECS UVLS helium discharging lamp at Fudan University. All the data were taken with SCIENTA R4000 electron analyzers; the overall resolution is set to 6 meV or better and the typical angular resolution is 0.3° . The samples were cleaved *in situ*, and measured under ultra-high vacuum, so that the aging effects are negligible in the data.

The general electronic structure of $\text{NaFe}_{0.9825}\text{Co}_{0.0175}\text{As}$ is rather similar to the well studied NaFeAs [22–24]. Figure 1(c) shows the photoemission intensity map near E_F taken at 7 K with 21.2 eV photons. There are a hole pocket and a small

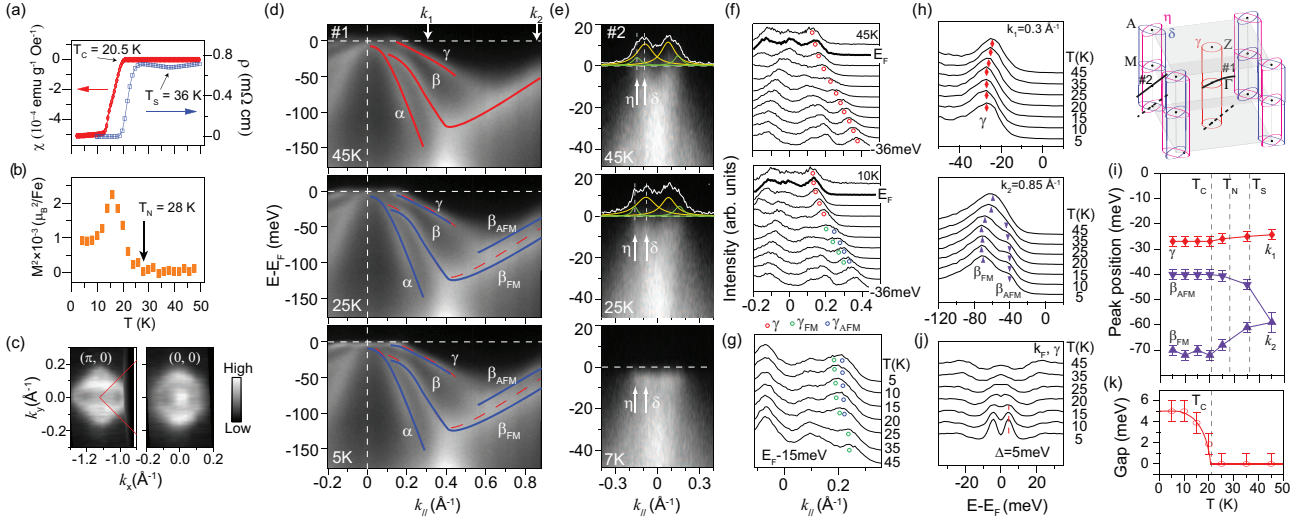


FIG. 1: (color online) (a) Magnetic susceptibility of $\text{NaFe}_{0.9825}\text{Co}_{0.0175}\text{As}$ single crystal taken at a magnetic field of 20 Oe in the zero field cool mode, and its resistivity as a function of temperature. (b) Temperature dependence of the magnetic order parameter at $Q = (1, 0, 1.5)$ for $\text{NaFe}_{0.9825}\text{Co}_{0.0175}\text{As}$ as measured by neutron scattering. (c) Photoemission intensity map at the Fermi energy integrated over $[E_F - 5 \text{ meV}, E_F + 5 \text{ meV}]$. (d) The band structure of $\text{NaFe}_{0.9825}\text{Co}_{0.0175}\text{As}$ at 45, 25, and 5 K respectively along cut #1 across Γ as indicated in the inset. The dashed lines in the lower panels are the band dispersion at 45 K for comparison purpose. (e) Temperature dependence of the band structure around the zone corner along cut #2 as indicated in the inset. The MDCs (momentum distribution curves) at E_F are plotted on the 25 and 45 K data. Each MDC was fitted to four Lorentzians (overlaid yellow and green lines). (f) MDCs near the zone center at 45 and 10 K. (g) Temperature dependence of the MDC at $E_F - 15 \text{ meV}$ near the zone center. The positions of the γ band are marked in panels (f) and (g). (h) Temperature dependence of the EDCs (energy distribution curves) at selected momenta: $k_1 = 0.3 \text{ \AA}^{-1}$, and $k_2 = 0.85 \text{ \AA}^{-1}$ respectively as marked in panel (d). Due to the broad lineshape, γ_{AFM} and γ_{FM} are not resolved, but the shift of the overall features is obvious. (i) The temperature dependence of the peak positions in panel (h). (j) The temperature dependence of the symmetrized EDCs measured at the k_F of γ . (k) The temperature dependence of the superconducting (SC) gap of γ . The gap size is estimated through an empirical fit as described in detail in Ref. [28]. The inset on the top right corner shows the Fermi surface of $\text{NaFe}_{0.9825}\text{Co}_{0.0175}\text{As}$. The two solid lines mark cut #1 and cut #2 along which the data in panels (d) and (e) are located, respectively. The two dashed lines on the bottom plane are their projections. The photoemission data in panels (c) and (e) were acquired in-house, and others were collected at SSRL.

patch-like feature point around $\Gamma (0, 0)$, and two orthogonal elliptical pockets around the zone corner. The photoemission intensity along cut #1 across Γ is plotted in Fig. 1(d), where three bands, α , β and γ could be resolved, but only γ crosses E_F and gives the hole Fermi surface. The band top of α is just below E_F , and contributes to the small patch in the zone center. Figure 1(e) plots the photoemission intensities at the zone corner, where two electron-like bands, δ and η , could be observed. As previous photon energy dependent study has revealed the negligible k_z dispersion of NaFeAs [23], the overall Fermi surface topology of $\text{NaFe}_{0.9825}\text{Co}_{0.0175}\text{As}$ is summarized in the inset on the top right corner of Fig. 1.

The signature of SDW on the electronic structure has been extensively studied before [22, 24–26], which is mainly manifested as a remarkable band reconstruction. As shown in Fig. 1(d), β shifts significantly with decreased temperature. To illustrate the subtle band reconstruction of γ , Fig. 1(f) plots the momentum distribution curves (MDCs) near the Fermi crossing of γ at several binding energies near E_F at 45 and 10 K, and Fig. 1(g) plots the MDC at $E_F - 15 \text{ meV}$ as a function of temperature. It is clear that γ first shifts in one direction due to the SDW [24], and then splits into two at low temperatures. Our recent ARPES study on the mechanically de-

twinning NaFeAs has shown that the β and γ bands disperse differently along the ferromagnetic (FM) and AFM directions, which gives an appearance of band splitting in the twinned sample here as noted by the subscripts in Fig. 1 [24]. Similar reconstruction effects can be observed in the energy distribution curves (EDCs) as well in Fig. 1(h). As shown by the temperature dependence of the EDC peak positions summarized in Fig. 1(i), the electronic structure reconstruction occurs above the structural transition due to the fluctuations of the SDW and electronic structure nematicity [24, 27]. It evolves smoothly across the structural and Neel transitions, and saturates below 20 K, with the separation of β_{AFM} and β_{FM} reaching 32 meV and the shift of γ reaching 3 meV. The reconstruction of δ and η is subtle, nevertheless in Fig. 1(e), their features in the MDCs at E_F clearly show finite shifts as well [24]. On the other hand, SC gap opens just below T_c , as illustrated by the symmetrized EDCs of the γ band with respect to E_F in Fig. 1(j) and the fitted SC gap in Fig. 1(k). The fact that the signatures of both the superconductivity and SDW emerge in the same band structure confirms their intrinsic coexistence. Furthermore, the band reconstruction due to SDW mainly occurs over a large energy and momentum scales for β below E_F , and it leaves the states on all the Fermi surfaces

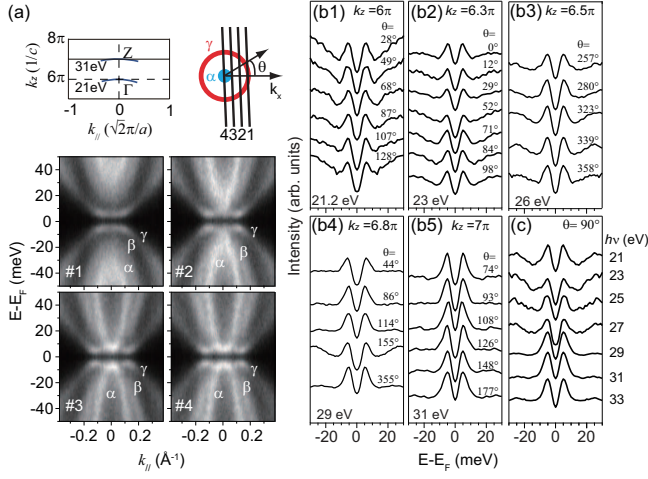


FIG. 2: (color online) (a) The photoemission intensities taken with 21.2 eV photons at 7 K near the zone center as shown by cuts #1 – #4 in the inset. The inset to the left shows the momentum cuts sampled by the 21 and 31 eV photons in the $k_x - k_z$ cross-section of the extended Brillouin zone. (b) The symmetrized spectra at the marked polar angles on the γ Fermi surface measured at five typical k_z values with (b1) 21.2, (b2) 23, (b3) 26, (b4) 29, and (b5) 31 eV photons. (c) k_z dependence of the symmetrized spectra measured on the γ Fermi surface of another sample at $\theta = 90^\circ$. The 21.2 eV data were collected at 7 K with a helium lamp, while the others were collected at 1 K at BESSY.

largely intact in this doping regime, therefore superconductivity could occur in the presence of SDW here.

The SC gap is mapped out extensively over the entire Brillouin zone. Figure 2(a) shows the symmetrized photoemission intensity along four momentum cuts across the γ hole Fermi surface in the $k_z = 6\pi$ plane. The suppression of the spectral weight around E_F indicates the opening of the SC gap. In Fig. 2(b1), the symmetrized EDCs along the γ pocket clearly show sharp coherent peaks, and SC gaps of similar amplitude. Data from other k_z planes in Figs. 2(b2)-2(b5), and data from another sample taken with more photon energies in Fig. 2(c) show that the gap is isotropically 5 meV on the γ pocket, as also summarized in Fig. 4(a).

Now we turn to the SC gap on the electron Fermi surfaces around the zone corner. Figure 3(a) shows symmetrized photoemission intensity for six momentum cuts across the δ/η pockets in the $k_z = 6\pi$ plane, where the SC gap opens on both Fermi surfaces. Collecting the symmetrized EDCs at various k_F 's along the δ pocket, Fig. 3(b1) demonstrates an anisotropic gap distribution, where the gap is about 7 meV in the flat part of the ellipse, and significantly drops to 4 meV near $\theta = 0^\circ, 180^\circ$. Moreover, such a behavior is observed for all five sampled k_z 's as shown in Figs. 3(b1)-3(b5). Similarly, such an anisotropic gap distribution is observed for η but rotated by 90° [Figs. 3(c1)-3(c5)]. The weak k_z dependence is further illustrated with more data taken at $k_z = 5.5\pi, 6.3\pi$, and 6.5π with 21, 28, and 30 eV photons respectively in the supplementary material [Fig. S1].

The gap distribution of $\text{NaFe}_{0.9825}\text{Co}_{0.0175}\text{As}$ is summarized in Figs. 4(a)-4(c). The gaps along the γ hole Fermi surface show isotropic distribution, while the gaps on the δ and η pockets vary significantly from 4 to 7 meV. As a comparison, Figures 4(d)-4(e) show the isotropic in-plane gap distribution on individual Fermi surfaces for an SDW-free $\text{NaFe}_{0.955}\text{Co}_{0.045}\text{As}$ sample ($T_c = 20$ K), which are retrieved from the symmetrized EDCs provided in the supplementary material [Fig. S2]. The gap is about 5 meV on the hole pocket, and 5.4 meV on the electron pockets. Such an isotropic in-plane gap distribution has been observed before in $\text{NaFe}_{0.95}\text{Co}_{0.05}\text{As}$ as well [29]. Furthermore, Fig. 4(f) compares both the Fermi surfaces and the SC gap distributions of $\text{NaFe}_{0.9825}\text{Co}_{0.0175}\text{As}$ and $\text{NaFe}_{0.955}\text{Co}_{0.045}\text{As}$. The hole pocket of $\text{NaFe}_{0.955}\text{Co}_{0.045}\text{As}$ is slightly smaller as expected from cobalt doping, and the ellipticity of its electron pockets is smaller as well.

So far in ARPES experiments, the in-plane anisotropy of SC gap has been observed only for LiFeAs [30, 31], $\text{Fe}(\text{Te},\text{Se})$ [32], KFe_2As_2 [33], and $\text{Ba}_{1-x}\text{K}_x\text{Fe}_2\text{As}_2$ [34] among all the iron-based superconductors, but none of them is in the coexisting regime. The small gap anisotropy on one of the hole pockets of $\text{Ba}_{1-x}\text{K}_x\text{Fe}_2\text{As}_2$ is within the experimental error that less than 0.6 meV difference over the 9~10 meV gap amplitude is observed [34]. The moderately anisotropic gap on a hole Fermi surface of LiFeAs might be a mere consequence of the Fermi surface topology, since it is qualitatively consistent with the gap function $\Delta(k) = \Delta_0 \cos k_x \cos k_y$ predicted based on the s^{+-} pairing symmetry [30, 31]. For $\text{NaFe}_{0.9825}\text{Co}_{0.0175}\text{As}$, the large ellipticity gives a variation of $|\cos k_x \cos k_y|$ from ~ 0.98 in the flat region to ~ 0.91 on the tip, which could not explain the over 40% change of the gap based on the Fermi surface topology. We note that an anisotropic gap distribution around the zone corner has also been revealed in LiFeAs , which deviates from the canonical s^{+-} -wave gap function and was explained in terms of the band hybridization [31]. Consistently, the deviation there is most prominent around $\theta = 45^\circ$ where the hybridization is the strongest. However, the anisotropic behavior in $\text{NaFe}_{0.9825}\text{Co}_{0.0175}\text{As}$ deviates the gap function remarkably around $\theta = 0$ and 90° , which is away from Fermi surface region of mixed orbital character. For $\text{Fe}(\text{Te},\text{Se})$, the anisotropy of the SC gap on the hole pocket was suggested to be a consequence of sizable second-nearest-neighbor interactions, while the anisotropic and nodal gap on a hole pocket of KFe_2As_2 may be related to strong intra-pocket scattering [35], or specific orbital characters near Z [28]. Alternatively, the angular variation in the d_{xy} orbital content of the γ Fermi surface was predicted to cause anisotropic gap distribution on the electron pockets [35]. However, since $\text{NaFe}_{0.9825}\text{Co}_{0.0175}\text{As}$ and $\text{NaFe}_{0.955}\text{Co}_{0.045}\text{As}$ have similar Fermi surface, orbital characters and interaction parameters, $\text{NaFe}_{0.955}\text{Co}_{0.045}\text{As}$ would have exhibited anisotropic gap if these had been the causes here. Therefore, the highly anisotropic gap distribution on the electron pockets of $\text{NaFe}_{0.9825}\text{Co}_{0.0175}\text{As}$ is most likely a direct consequence of the coexisting SDW.

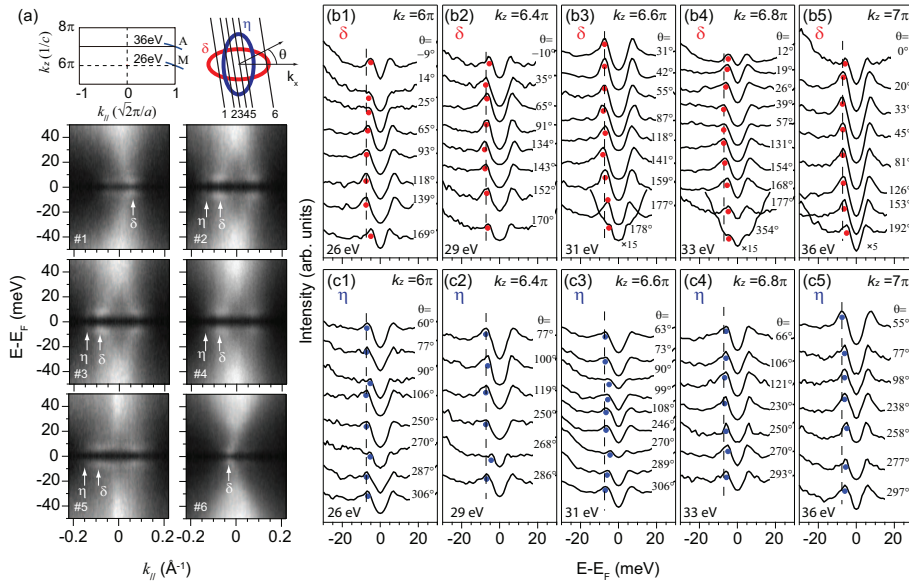


FIG. 3: (color online) (a) The photoemission intensities taken with 26 eV photons at 1 K near the zone corner as shown by cuts #1 – #6 in the top-right inset. The top-left inset shows the momentum cuts sampled by the 26 and 36 eV photons in the $k_x - k_z$ cross-section of the Brillouin zone. (b) The symmetrized spectra at the marked polar angles on the δ Fermi surface measured at five typical k_z 's with (b1) 26, (b2) 29, (b3) 31, (b4) 33, and (b5) 36 eV photons. The dashed lines here are guides to the eyes for the variation of the SC gaps. (c1)-(c5) Same as in panels (b1)-(b5) but on the η electron Fermi surface. All data were collected at 1 K in BESSY-II. Note that the bottom curves in panels (b3), (b4), and (b5) are magnified vertically.

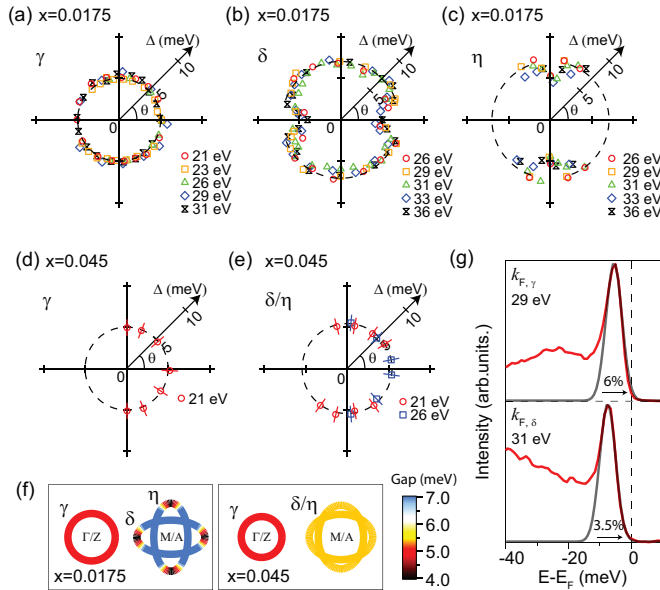


FIG. 4: (color online) Polar plots of the SC gap for the (a) γ , (b) δ and (c) η Fermi surfaces of $\text{NaFe}_{0.9825}\text{Co}_{0.0175}\text{As}$, respectively. The polar angle θ follows the same definition in Figs. 2 and 3. The error bar for the gaps is ± 1 meV based on the fitting. Polar plots of the SC gap of $\text{NaFe}_{0.955}\text{Co}_{0.045}\text{As}$ for the (d) γ , and (e) δ/η Fermi surfaces respectively. (f) False-color plots of the gap distribution on the Fermi surfaces of $\text{NaFe}_{0.9825}\text{Co}_{0.0175}\text{As}$ and $\text{NaFe}_{0.955}\text{Co}_{0.045}\text{As}$. (g) The typical spectra at the Fermi crossings of the γ and δ bands taken at 1 K in BESSY-II. The intensity ratio of the residual spectral weight at E_F is referred to the coherence peak height. Two Gaussians with 6 meV full-width-half-maximum are overlaid.

Theories based on the s^{++} pairing symmetry have suggested the nodeless and anisotropic gap distribution in the presence of weak SDW [15, 16]. Consistently, compared with NaFeAs [24], much weaker SDW order is present in $\text{NaFe}_{0.9825}\text{Co}_{0.0175}\text{As}$: the band folding due to the SDW order

is negligible, and no SDW gap induced by the hybridization with the folded bands is observed here. In a recent theoretical study, it was predicted that even weak SDW order will cause appreciable gap anisotropy [16]. Particularly, it was found that the gap at the tip region of the electron Fermi surface is smaller than that at the flat region, in good agreement with our observation. Furthermore, the observed nodeless SC gap disallows the pairing mechanism based on the s^{++} pairing symmetry that predicts SC gap nodes in the SDW state [9, 15].

The prominent band reconstruction of β observed here with a 32 meV separation between the dispersions along the AFM and FM directions is smaller than the 46 meV observed in NaFeAs [22]. Such a band reconstruction energy scale is distinct at a specific doping, and is correlated with the SDW transition temperature as observed in $\text{Sr}_{1-x}\text{K}_x\text{Fe}_2\text{As}_2$ [13]. Therefore, the sharp band dispersion with a single set of band reconstruction energy scale, plus the resolution limited width of the superconducting coherent peak [Fig. 4(g)], highlight the homogeneous nature of the electronic state in the momentum space. Moreover, although the shielding fraction of the bulk sample is 75% based on our susceptibility measurements, the ARPES data are taken on a small region ($0.05 \text{ mm} \times 0.2 \text{ mm}$) of the cleaved surface. As shown in Fig. 4(g), the photoemission intensity at E_F in the superconducting state is negligible, which suggests the absence of non-superconducting region. That is, there is no phase separation of superconducting regions and non-superconducting SDW regions in the coexisting phase. Our results thus rule out the appearance of macroscopic phase separation and further support the intrinsic coexistence. These are consistent with a recent STM study on the coexisting phase of $\text{NaFe}_{1-x}\text{Co}_x\text{As}$ ($x=0.014$) [21], where the coexistence was found to occur microscopically in an anti-correlated but non-exclusive way between the two orders. Such a non-exclusive coexistence can be understood based on our observation of the indirect competition between SDW and superconductivity in the electronic structure.

Note that, the energy scales observed in STM for both the “SDW gap” feature (~ 17 meV, and it should be a momentum-integrated effect of the band reconstruction) and SC coherence peak (~ 5 meV) are quite independent of space. This is further consistent with the single set of SDW/SC energy scales observed here by ARPES.

Our neutron scattering data on the same sample reveals that static antiferromagnetic long-range order coexists with superconductivity, similar to the static antiferromagnetic order/superconductivity coexisting $\text{BaFe}_{2-x}\text{Ni}_x\text{As}_2$ samples [14]. The intensity of the SDW diffraction peak decreases upon entering the SC state, suggesting a competition between the two orders [Fig. 1(b)]. The magnitude of the SDW order could be monitored directly from the energy scale of the band reconstruction. However, we did not observe any remarkable change of band reconstruction below T_c , which suggests that the competition between the two orders does not affect the magnitude of the local SDW order at the fast time scale of photoemission (~ 1 fs). Alternatively, since the itinerant electrons near E_F could play an important role in stabilizing the long-range SDW order [36], when the SC gap opens, the coherence of SDW order could be suppressed. Consequently, the enhanced fluctuation of the local SDW order could be responsible for the observed suppression of the effective (or time-averaged) moment at the quasi-elastic neutron scattering time scale ($\gg 1$ ps) [37].

To summarize, we have revealed detailed electronic structure in the superconductivity/SDW coexisting regime of $\text{NaFe}_{1-x}\text{Co}_x\text{As}$ ($x=0.0175$), and signature in the momentum space for the intrinsic microscopic coexistence. We found that SDW does not cause a noticeable depletion of the states at the Fermi energy, which allows the superconductivity to emerge. Therefore, it explains why the two orders could coexist in a non-exclusive way. Moreover, we show that the anisotropy of the SC gap on the electron pockets is likely a distinct consequence of the coexisting SDW order, while the absence of gap node puts strong constraints on the pairing symmetry in theory of iron-based superconductors.

We gratefully acknowledge the helpful discussions with Prof. J. P. Hu and Prof. A. V. Chubukov, and the experimental support by Dr. D. H. Lu, Dr. M. Hashimoto at SSRL, and Dr. E. Rienks at BESSY II. This work is supported in part by the National Science Foundation of China and National Basic Research Program of China (973 Program) under the grant Nos. 2012CB921400, 2011CB921802, 2011CBA00112. The single crystal growth efforts and neutron scattering work at University of Tennessee are supported by the US DOE, BES, through contract DE-FG02-05ER46202. SSRL is operated by the US DOE, BES, Divisions of Chemical Sciences and Material Sciences.

* Electronic address: dlfeng@fudan.edu.cn

[1] M. R. Norman, *Science* **332**, 196 (2011).

- [2] D. J. Scalapino, *Rev. Mod. Phys.* **84**, 1383 (2012)
- [3] F. Steglich, J. Aarts, C. D. Bredl, W. Lieke, D. Meschede, W. Franz, H. Schäfer, *Phys. Rev. Lett.* **43**, 1892 (1979).
- [4] P. Limelette, P. Wzietek, S. Florens, A. Georges, T. A. Costi, C. Pasquier, D. Jérôme, C. Mézière, and P. Batail, *Phys. Rev. Lett.* **91**, 016401 (2003).
- [5] Y. Kamihara, T. Watanabe, M. Hirano, and H. Hosono, *J. Am. Chem. Soc.* **130**, 3296 (2008).
- [6] X. H. Chen, T. Wu, G. Wu, R. H. Liu, H. Chen, and D. F. Fang, *Nature (London)* **453**, 761 (2008).
- [7] C. de la Cruz, Q. Huang, J. W. Lynn, J. Li, W. Ratcliff II, J. L. Zarestky, H. A. Mook, G. F. Chen, J. L. Luo, N. L. Wang, and P. C. Dai, *Nature (London)* **453**, 899 (2008).
- [8] D. K. Pratt, W. Tian, A. Kreyssig, J. L. Zarestky, S. Nandi, N. Ni, S. L. Budko, P. C. Canfield, A. I. Goldman, and R. J. McQueeney, *Phys. Rev. Lett.* **103**, 087001 (2009).
- [9] R. M. Fernandes *et al.*, *Phys. Rev. B* **81**, 140501R (2010).
- [10] D. R. Parker, M. J. P. Smith, T. Lancaster, A. J. Steele, I. Franke, P. J. Baker, F. L. Pratt, M. J. Pitcher, S. J. Blundell, and S. J. Clarke, *Phys. Rev. Lett.* **104**, 057007 (2010).
- [11] C. Lester, J.-H. Chu, J. G. Analytis, T. G. Perring, I. R. Fisher, and S. M. Hayden, *Phys. Rev. B* **81**, 064505 (2010).
- [12] S. Avci *et al.* *Phys. Rev. B* **83**, 172503 (2011).
- [13] Y. Zhang *et al.*, *Phys. Rev. Lett.* **102**, 127003 (2009).
- [14] H. Q. Luo, R. Zhang, M. Laver, Z. Yamani, M. Wang, X. Y. Lu, M. Y. Wang, Y. C. Chen, S. Li, S. Chang, J. W. Lynn, and P. C. Dai, *Phys. Rev. Lett.* **108**, 247002 (2012).
- [15] D. Parker, M. G. Vavilov, A. V. Chubukov, and I. I. Mazin, *Phys. Rev. B* **80**, 100508(R) (2009).
- [16] S. Maiti, R. M. Fernandes, and A. V. Chubukov, *Phys. Rev. B* **85**, 144527 (2012).
- [17] J. P. Reid *et al.*, arXiv:1105.2232 (unpublished).
- [18] M.-H. Julien, H. Mayaffre, M. Horvatic, C. Berthier, X. D. Zhang, W. Wu, G. F. Chen, N. L. Wang, and J. L. Luo, *EPL* **87**, 37001 (2009)
- [19] Y. Laplace, J. Bobroff I, F. Rullier-Albenque, D. Colson, and A. Forget, *Phys. Rev. B* **80**, 140501(R) (2009)
- [20] X. Zhou, P. Cai, A. Wang, W. Ruan, C. Ye, X. Chen, Y. You, Z.-Y. Weng, and Y. Wang, *Phys. Rev. Lett.* **109**, 037002 (2012).
- [21] P. Cai, X. Zhou, W. Ruan, A. Wang, X. Chen, D.-H. Lee, Y. Wang, arXiv:1208.3842v1 (unpublished).
- [22] C. He *et al.*, *Phys. Rev. Lett.* **105**, 117002 (2010).
- [23] C. He *et al.*, *J. Phys. Chem. Solids* **72**, 479 (2011).
- [24] Y. Zhang *et al.*, *Phys. Rev. B* **85**, 085121 (2012).
- [25] M. Yi, D. H. Lu, R. G. Moore, K. Kihou, C.-H. Lee, A. Iyo, H. Eisaki, T. Yoshida, A. Fujimori, Z.-X. Shen, *New Journal of Physics* **14**, 073019 (2012).
- [26] L. X. Yang *et al.*, *Phys. Rev. Lett.* **102**, 107002 (2009).
- [27] S. Kasahara *et al.*, *Nature* **486**, 382 (2012).
- [28] Y. Zhang, Z. R. Ye, Q. Q. Ge, F. Chen, J. Jiang, M. Xu, B. P. Xie, and D. L. Feng, *Nat. Phys.* **8**, 371 (2012).
- [29] Z.-H. Liu *et al.*, *Phys. Rev. B* **84**, 064519 (2011).
- [30] S. V. Borisenko, V. B. Zabolotnyy, A. A. Kordyuk, D. V. Evtushinsky, T. K. Kim, I. V. Morozov, R. Follath, B. Büchner, *Symmetry* **4**, 251 (2012).
- [31] K. Umezawa *et al.*, *Phys. Rev. Lett.* **108**, 037002 (2012).
- [32] K. Okazaki *et al.*, *Phys. Rev. Lett.* **109**, 237011 (2012).
- [33] K. Okazaki *et al.*, *Science* **337**, 1314 (2012)
- [34] D. V. Evtushinsky *et al.*, *Phys. Rev. B* **79**, 054517 (2009)
- [35] F. Wang, H. Zhai, D. H. Lee, *Phys. Rev. B* **81**, 184512 (2010).
- [36] M. D. Johannes and I. I. Mazin, *Phys. Rev. B* **79**, 220510(R) (2009).
- [37] P. Vilmercati *et al.*, *Phys. Rev. B* **85**, 220503(R) (2012).

**Supplementary material for: Anisotropic but nodeless superconducting gap
in the presence of spin density wave in iron-pnictide superconductor**

$\text{NaFe}_{1-x}\text{Co}_x\text{As}$

Q. Q. Ge (葛青亲),¹ Z. R. Ye (叶子荣),¹ M. Xu (徐敏),¹ Y. Zhang (张焱),¹ J. Jiang (姜娟),¹ B. P. Xie (谢斌平),¹ Y. Song (宋宇),² C. L. Zhang (张承林),² P. C. Dai (戴鹏程),^{2,3} and D. L. Feng (封东来)^{1,*}

¹*State Key Laboratory of Surface Physics, Department of Physics,
and Advanced Materials Laboratory, Fudan University,
Shanghai 200433, People's Republic of China*

²*Department of Physics and Astronomy,
The University of Tennessee, Knoxville, Tennessee 37996-1200, USA*

³*Beijing National Laboratory for Condensed Matter Physics,
Institute of Physics, Chinese Academy of Sciences, Beijing 100190, China*

(Dated: July 28, 2021)

Abstract

In this supplementary material, we present additional symmetrized EDCs for the comprehensive survey of the superconducting gap in $\text{NaFe}_{0.9825}\text{Co}_{0.0175}\text{As}$ and $\text{NaFe}_{0.955}\text{Co}_{0.045}\text{As}$.

PACS numbers: 74.25.Jb,74.70.Xa,79.60.-i,71.20.-b

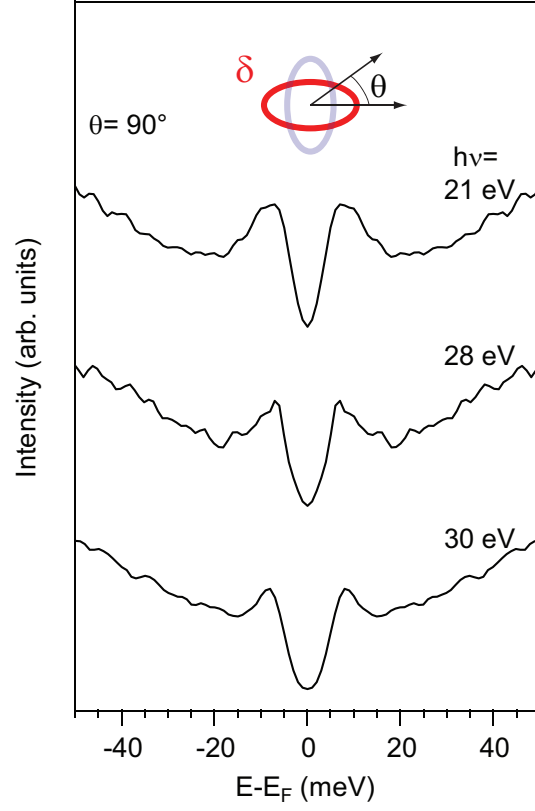


FIG. S1: **Symmetrized EDCs on the δ electron pocket in $\text{NaFe}_{0.9825}\text{Co}_{0.0175}\text{As}$.** The symmetrized EDCs are measured at three different k_z 's, 5.5π (21 eV), 6.3π (28 eV), and 6.5π (30 eV) on the δ electron pocket. The superconducting gap on the δ electron pocket shows weak k_z dependence for $\text{NaFe}_{0.9825}\text{Co}_{0.0175}\text{As}$.

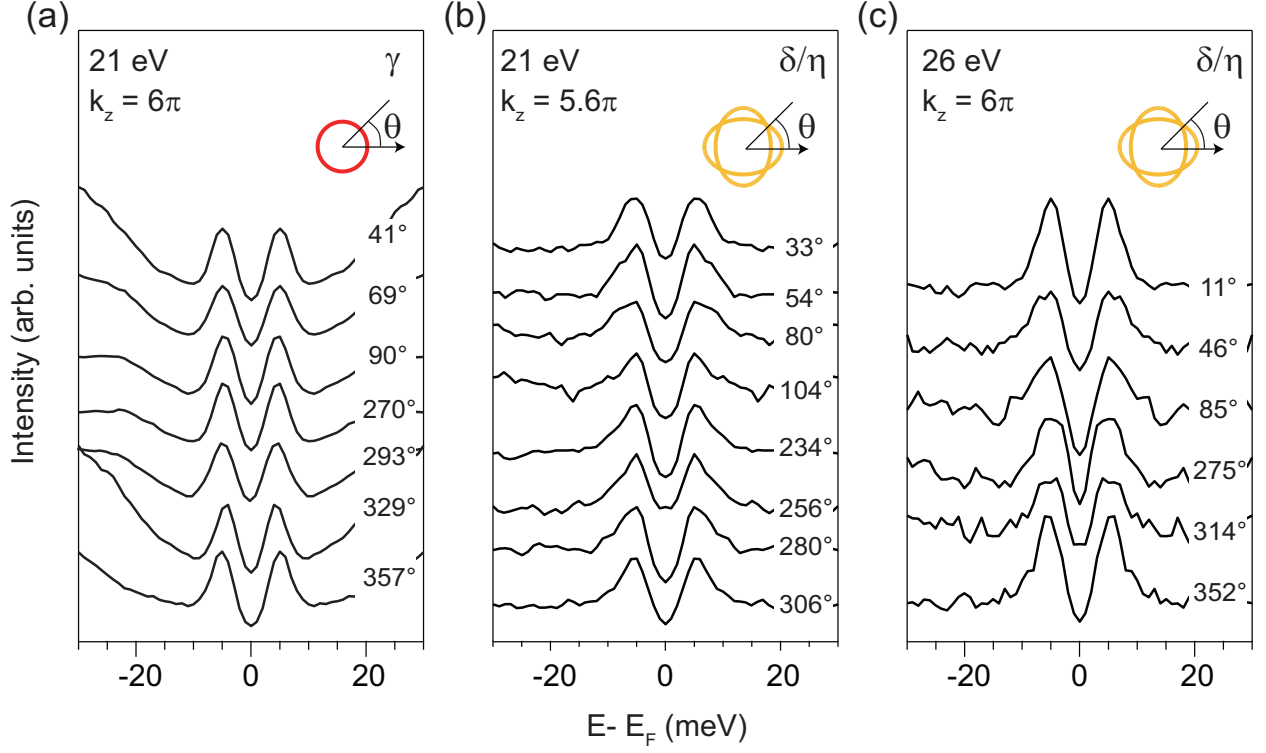


FIG. S2: **Symmetrized EDCs on the hole and electron pockets in $\text{NaFe}_{0.955}\text{Co}_{0.045}\text{As}$, corresponding to the data in Figs. 4(d) and 4(e) in the main text.** (a) The symmetrized EDCs along the γ Fermi surface at $k_z = 6\pi$. (b) and (c) The symmetrized EDCs on the δ/η electron Fermi surfaces at $k_z = 5.6\pi$ and 6π , respectively. The superconducting gap magnitudes were determined by fitting the symmetrized EDCs with a typical superconducting-state spectral function [1]. The superconducting gaps on the hole and electron Fermi surfaces are nodeless and isotropic for the SDW-free $\text{NaFe}_{0.955}\text{Co}_{0.045}\text{As}$. Note that, since the Fermi crossings of δ and η are very close in $\text{NaFe}_{0.955}\text{Co}_{0.045}\text{As}$, we did not plot the symmetrized EDCs separately here for these two Fermi surfaces.

* Electronic address: dlfeng@fudan.edu.cn

[1] M. R. Norman, M. Randeria, H. Ding, and J. C. Campuzano, Phys. Rev. B **57**, R11093 (1998).